SANDIA REPORT
SAND2017-10219
Unlimited Release
Printed November 2017

Measurements of pore-scale flow through apertures

Kirsten Chojnicki

Prepared by
Sandia National Laboratories
Albuquerque, New Mexico 87185 and Livermore, California 94550

Sandia National Laboratories is a multimission laboratory managed and operated by National Technology and Engineering Solutions of Sandia, LLC, a wholly owned subsidiary of Honeywell International, Inc., for the U.S. Department of Energy's National Nuclear Security Administration under contract DE-NA0003525.

Issued by Sandia National Laboratories, operated for the United States Department of Energy by National Technology and Engineering Solutions of Sandia, LLC.

Available to DOE and DOE contractors from
U.S. Department of Energy
Office of Scientific and Technical Information
P.O. Box 62
Oak Ridge, TN 37831

Telephone: (865) 576-8401
Facsimile: (865) 576-5728
E-Mail: reports@osti.gov
Online ordering: http://www.osti.gov/scitech

Available to the public from
U.S. Department of Commerce
National Technical Information Service
5301 Shawnee Rd
Alexandria, VA 22312

Telephone: (800) 553-6847
Facsimile: (703) 605-6900
E-Mail: orders@ntis.gov
Online order: https://classic.ntis.gov/help/order-methods/

SAND201X-XXXX
Printed September 2017
Unlimited Release

Measurements of pore-scale flow through apertures

Kirsten Chojnicki
Geotechnology & Engineering
Sandia National Laboratories
P. O. Box 5800
Albuquerque, New Mexico 87185-MS0750

Abstract

Pore-scale aperture effects on flow in pore networks was studied in the laboratory to provide a parameterization for use in transport models. Four cases were considered: regular and irregular pillar/pore alignment with and without an aperture. The velocity field of each case was measured and simulated, providing quantitatively comparable results. Two aperture effect parameterizations were considered: permeability and transmission. Permeability values varied by an order of magnitude between the cases with and without apertures. However, transmission did not correlate with permeability. Despite having much greater permeability the regular aperture case permitted less transmission than the regular case. Moreover, both irregular cases had greater transmission than the regular cases, a difference not supported by the permeabilities. Overall, these findings suggest that pore-scale aperture effects on flow though a pore-network may not be adequately captured by properties such as permeability for applications that are interested in determining particle transport volume and timing.

ACKNOWLEDGMENTS

The author gratefully acknowledges Jason Heath for conducting the numeric simulations and Martin Nemer for laboratory access and the use of the microscope and high speed camera.

TABLE OF CONTENTS

FIGURES

TABLES

1. INTRODUCTION

For underground nuclear tests, the large-scale transport of radionuclides through the subsurface is strongly influenced by processes occurring at the scale of the rock pores. These processes often cause changes in the pore network geometry that in turn affect the subsequent hydrodynamic and mechanical flow processes in a complex feedback process. Pore-scale apertures or fractures may be formed more often during some tests which may be an important process for radionuclide transport models to describe effectively when used for forensic or predicative purposes related to those events. One of the challenges in incorporating such effects into models is determining an appropriate way to parameterize them. Experiments herein have been designed to elucidate the pore-scale flow fields through apertures to provide a way to parameterize the effect of apertures on the flow for use in transport models.

2. EXPERIMENT DESIGN

To determine the effect of apertures on pore-scale flow, experiments were designed in pore networks with and without apertures such the aperture effect would be revealed by by comparison of the results.

2.1. Pore network geometry

Two common pore network parameterizations used in flow models were considered herein, a staggered (or regular) and a random (or irregular) alignment of the pillars (or grains) and pores. An aperture oriented ~45^{o} from the flow direction was chosen. The flow direction was from left to right in the pore networks. The reference to an aperture rather than a fracture signifies here that the pathway is lined with whole rather than broken grains/pillars. These choices resulted in the 4 pore network configurations shown schematically in Figure 1.

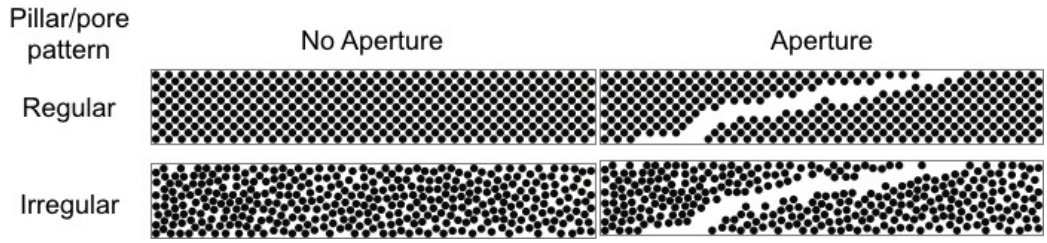

Figure 1 Schematic showing the four pore network configurations considered in this study.

Each pore network was made into a porous media chip (Dolomite Microfluidics), an example is shown in Figure 2. The pillars were chosen to be the diameter of large sand grains (900 μm) and the pore diameters were chosen to represent those that may appear in a loosely consolidated sand or tuff. The details of the pillar dimensions are shown in the inset in Figure 2.

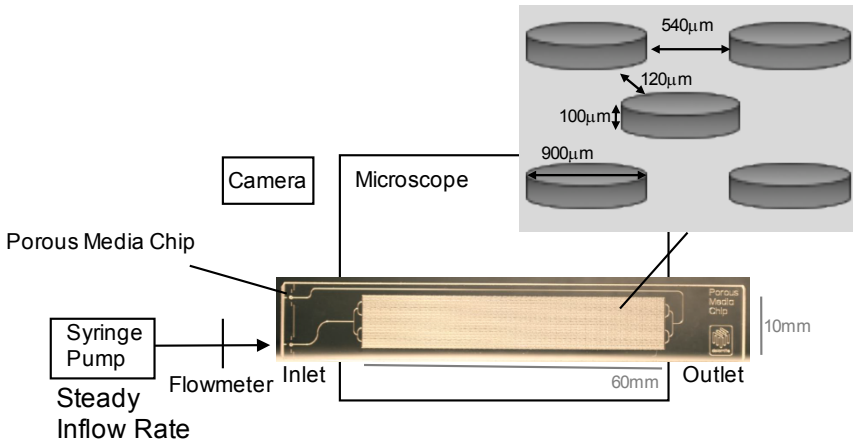

Figure 2 Schematic showing the porous media chip and the general experiment set up.

2.2. Fluid flow

Fluid flow was generated through the chip using a syringe pump (Harvard Apparatus PhD Ultra) held at a constant flow rate of 500 μL/min. This flowrate yielded a laminar flow with Re << 10, confirmed with velocity measurements of the chip entrance plane. The fluid passing through the chip was water containing small particles with a diameter of 1 μm (Bangs Industries). The density of the particles was matched to that of water to ensure the particles would travel as tracers within the fluid and not interfere with its motion. The pump was started and the flow was allowed to come to steady state before images of the flow were taken. A steady flow rate at the chip inlet was confirmed with a flowmeter inline with the flow that was located between the pump and the inlet of the chip.

2.3. Flow measurement

A microscope (Leica DM IRB microscope) with a 10x objective was used to magnify the particles such that they could be imaged using a CCD camera (Phantom Miro 4) connected to the microscope. A frame rate of 1200 frames per second (830 μs per frame) was used to ensure the particles were stopped during the image capture to prevent blurring of the particle image. The field of view was 600 x 800 pixels with a resolution of 0.02 mm/pixel measured using a reticle with 0.01 mm/division.

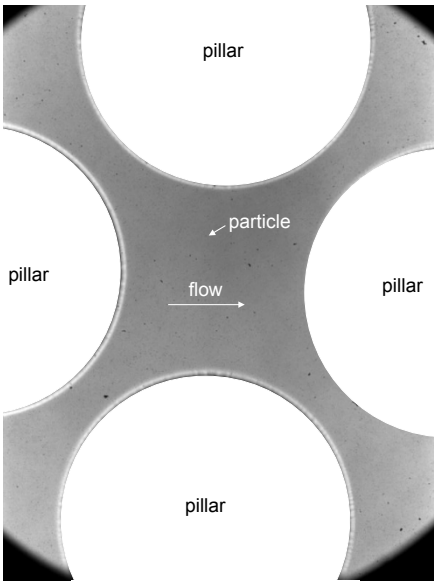

Figure 3 Example image of flowing particles.

The particle images were used to compute the velocity field of the flowing fluid using the particle image velocimetry (PIV) technique. In this technique a pair of particle images taken sequentially is analyzed using a cross correlation algorithm to determine the average displacement of the particle images during the time separating the image pair. The result is a non-invasive measurement of the velocity field. The images were taken in a vertical plane near the center of the chip ~50 μm from the bottom face. Thus, the flow represented by the images was along the centerline and away from the top and bottom faces of the chip. The program PIVlab, a Matlab application, was used to compute the cross correlation, provide some basic filtering of the results, and compute an average vector field over a record length of 1000 frames.

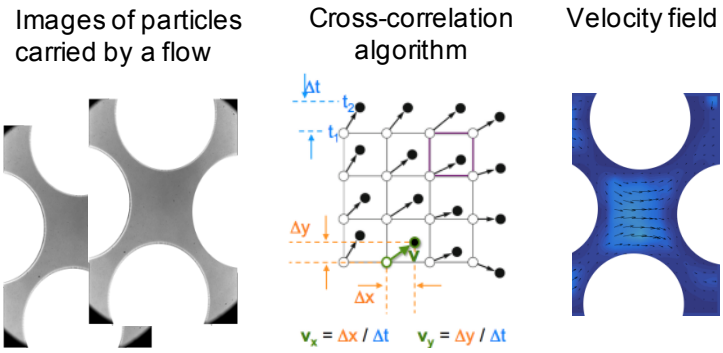

Figure 4 Schematic showing the steps involved in the particle image velocimetry (PIV) flow measurement technique.

3. RESULTS

3.1. Measured velocity fields

A position in the micromodel near the aperture inlet was chosen as a location of interest and velocity fields were measured there (see Figure 5). The results show that both aperture cases have faster maximum flow velocities (yellow regions in the colormap) in this pore space than the cases without apertures. The average velocity in the micromodel was computed as 6.0 mm/s, a value close to the measured values giving confidence that the PIV algorithm generated quantitatively relevant values.

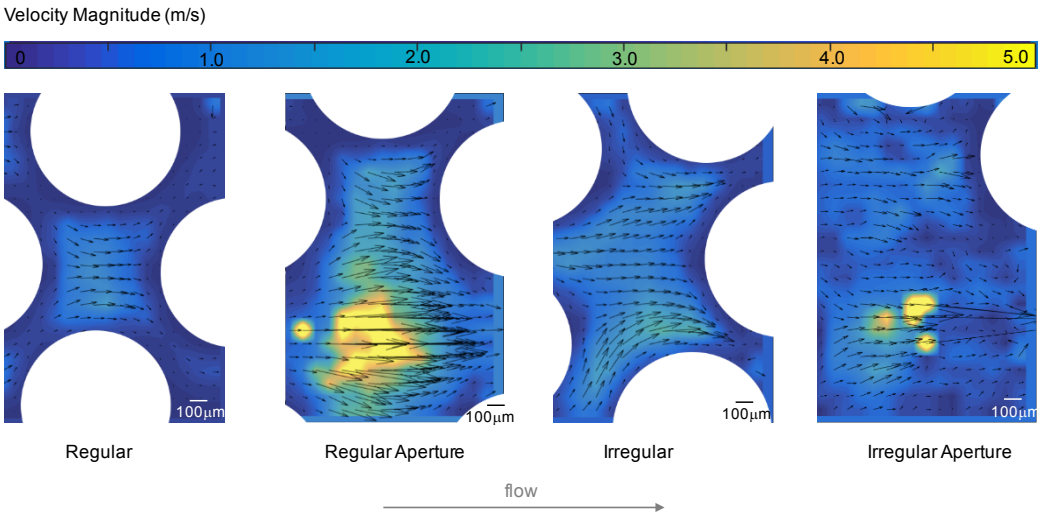

Figure 5 Measured velocity fields near the aperture inlet for all 4 cases. Arrows indicate local flow direction and length indicates magnitude. Colormap indicates velocity magnitude with fast flow in yellow.

3.2. Simulated velocity fields

Since it was not feasible to measure the entire flow field of all pore spaces, a model was used to calculate what the overall flow pattern would be in the chip. COMSOL was used to model the flow in 2D. The simulation domain patterns matched those in Figures 1 and 2. Laminar flow was modeled using Stokes flow (pressure gradient driven flow without inertial terms). A steady-state inlet volumetric flux was applied to the left side of the domain and an outflow boundary condition was applied to the right side. No-flow boundary conditions were applied to the top, bottom, front and back sides. Water was the fluid injected and it was injected at a rate of 500 µl/min, equal to the experimental flow.

Simulation results of the velocity field across the entire domain are shown in Figure 6. In the regular geometry, the case without an aperture (Figure 6a) had a fast flow path along the top and bottom boundaries of the flow. This flow pattern was unexpected as this case was expected to produce canonical pore scale flow with fast flow in the pore throats and slower flow in the pore bodies. This result may indicate that the distances between the top and bottom domain boundaries and the adjacent pillars is wide. Although unexpected, the result is interesting as it implies that situations where a flow

can chose to move *along* a pore network rather than *through* it, for example between a jacket and a sample in the lab or casing and cement sheath in a wellbore, will produce fast flow paths.

The regular geometry case with an aperture (Figure 6b) had a fast flow path through the aperture. In the irregular geometry, the case without an aperture (Figure 6c) did not have one continuous fast flow path but had disconnected segments of fast flow. The case with the aperture (Figure 6d) had the fastest flow path through the aperture. The apertures (Figure 6b,d) did not produce a flow path with fast flow the entire length but rather intermittent regions of fast flow (red).

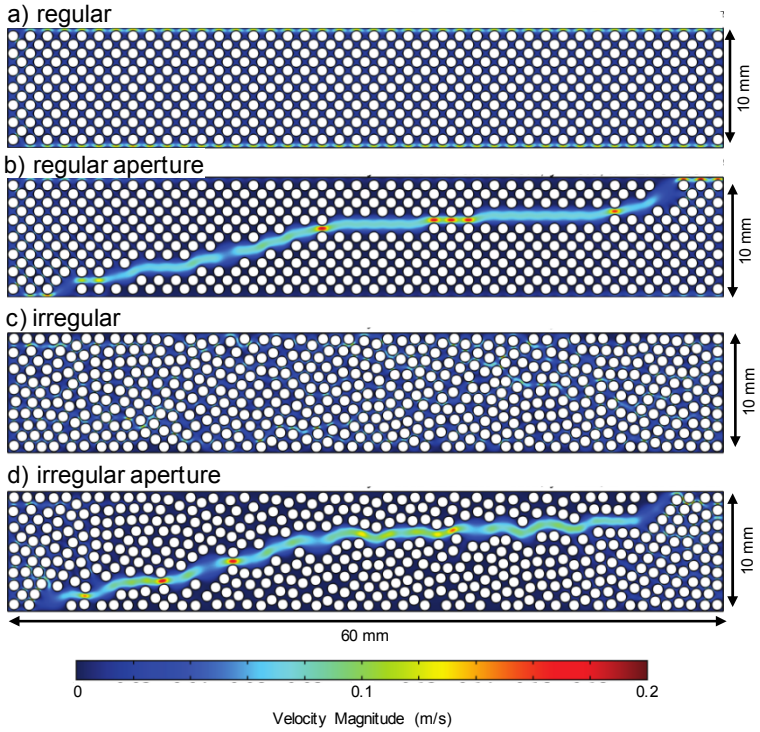

Figure 6 Simulated velocity fields in the entire micromodel. Flow is from left to right. Colormap indicates velocity magnitude with fast flow in red.

3.3. Comparison of simulated and measured velocity fields

To understand how the simulated velocity results compare with the measured velocity results, the simulation results in individual pore spaces were examined and compared with the measured velocity fields. A representative example of such a comparison is shown Figure 7. The whole simulated field of the regular aperture case (Figure 7a) is shown for context and the velocity field of the individual pore of interest (red box Figure 7a) is shown in Figure 7b. The measured velocity in the corresponding pore space is shown in Figure 7c. The maximum simulated velocity magnitude in the pore space (60 mm/s) was double the maximum measured velocity magnitude (30 mm/s). This may be explained by more losses that were present in the laboratory that were not accounted for in the simulation, for example losses due to variations with depth that were not modeled in the 2D flow scenario. Nevertheless, the velocities are of the same

order of magnitude suggesting the assumptions used in generating the simulation may be a reasonable description of the first order flow dynamics.

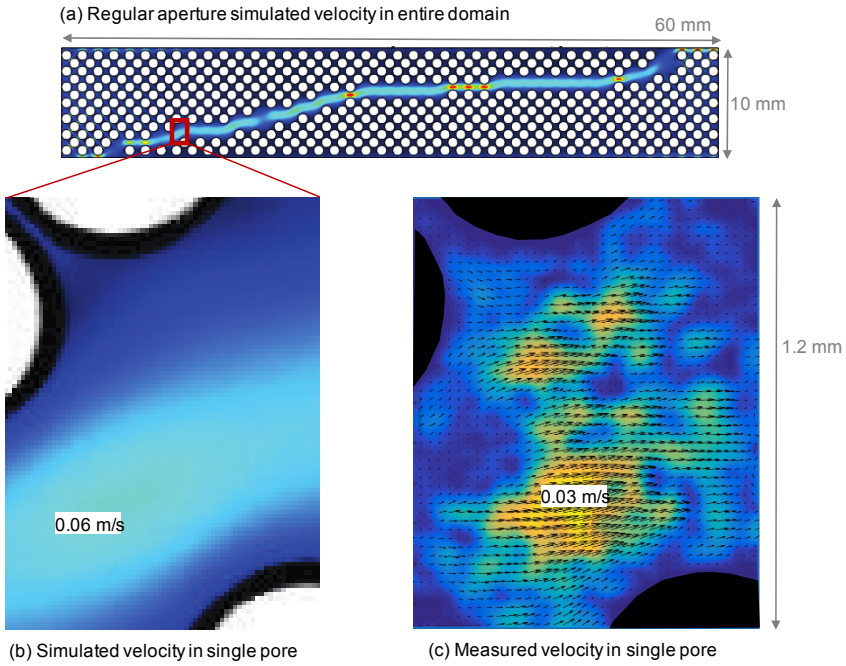

Figure 7 (a) Simulated velocity fields in the entire domain and (b) a single pore space compared with the (c) measured velocity for the same pore space.

4. APPROXIMATING APERTURE EFFECTS

To better understand the effects of the apertures on the flow two parameters were computed using the simulated flow fields, permeability and transmission. Simulated fields were used since the approximations used in the modeling were determined to capture the first order flow dynamics of the laboratory experiments (section 3.3).

4.1.1. Permeability

In the first parameterization, an effective permeability of the flow was calculated. Permeability is a parameter used in continuum-scale models to describe how well fluids travel through a pore network or other geometry. Permeability was calculated using Darcy's law,

$$q = \frac{Q}{A} = -\frac{k}{\mu}\nabla p$$

where q is the volumetric flux of the flow, Q is the volumetric flow rate, A is the cross sectional area normal to the flow direction, k is the permeability, μ is the dynamic viscosity of the fluid, and ∇p is the pressure gradient driving the flow. Results are listed in Table 1.

Table 1. Flow permeability

Case	k (m²)
Regular	8.05e-10
Regular Aperture	2.18e-9
Irregular	6.71e-10
Irregular Aperture	2.67e-9

The calculated permeabilities for the two cases with apertures are an order of magnitude larger than the two cases without apertures. These results suggest that one may be able to model the effects of the apertures by increasing the permeability by an order of magnitude when the apertures are present, assuming similar conditions to those assumed here. Those assumptions include that the aperture dimensions are comparable to the pore network dimensions, the aperture continues throughout the entire flow field, the aperture is oriented ~45° from the dominate flow direction, and the flow is laminar.

4.1.2. Transmission

An alternate way of thinking about the effects of the aperture on the flow, is the time over which tracers are transported by the flow. Neutrally-buoyant particles (N = 1500) with a diameter of 1 μm were added to the simulation as tracers. Tracers were injected uniformly along the inlet boundary. The percentage of the particles that reached the outflow boundary within 5 s was then calculated as the transmission, T, of the pore network, listed in Table 2.

Table 2. Transmission of tracer particles in 5 s

Case	T (%)
Regular	84
Regular Aperture	80
Irregular	87
Irregular Aperture	86

For the regular aperture case, the case *without* the aperture transmitted more particles (84%) than the case with the aperture (80%). In fact, the regular aperture case was lowest transmitting case considered. The irregular and irregular aperture cases transmitted similar numbers of particles (87% & 86%) and more particles than the regular and regular aperture cases.

It is interesting to note that the transmission values do not correlate with the permeability values. Although the regular aperture case has an order of magnitude greater permeability than the regular case (Table 1), it transmits 4% less particles (Table 2). Similarly, although the irregular and irregular aperture cases have an order of magnitude difference in permeability (Table 1), they transmit about the same number of particles (Table 2).

To better understand why there was a difference in transmission among the cases, the frequency distributions were then plotted for the travel times of the transmitted particles as shown in Figure 8. The distributions look quite different for each case. The case with the largest number of particles leaving at ~ 1 s was the regular aperture case (Figure 8a). This is likely because there are two fast flow paths in the regular case along the top and bottom boundaries where particles and the flow may encounter very little losses.

Both the cases with apertures (Figure 8b,d) have more particles leaving at early times (< 2s) that then taper off to 5s. However, there are more total particles that leave in early times in the irregular aperture case possibly leading to its larger transmission value. The regular aperture case (Figure 8a) has a bimodal distribution with its first and dominate peak at 1s and a secondary peak at ~ 4s. This case is the only case with a bimodal distribution. And finally, the regular aperture case (Figure 8c) has an apparently normal distribution centered ~ 2.8s. This case is interesting because there is an apparent delay of ~1s in the particles leaving the simulation domain compared with the other three cases; the distribution starts at ~2s rather than ~1s. Yet enough particles are moved at those later times to reach approximately the same transmission level as the irregular aperture case (Figure 8d).

Overall, the results presented in Figure 8 do not provide a clear understanding of the differences in transmission values among the cases. More work would need to be done understanding the relationship between travel time distributions and transmission and the core flow properties.

5. SUMMARY

Experiments were designed to elucidate the effects of pore-scale apertures on flow in pore networks to provide a way to parameterize the effect of apertures on the flow for use in transport models. Four configurations were considered with a regular (staggered) pillar (grain) and pore alignment (1) without and (2) with an aperture and an irregular pillar and pore alignment (3) without and (4) with an aperture. The velocity fields moving through these geometries were then measured using PIV and simulated in 2D with COMSOL, assuming steady state flow of water through the pore network. Simulated velocity fields were quantitatively comparable to measured velocity fields lending confidence to the assumptions made in the simulation, primarily that 2D flow is an adequate approximation of the laboratory flow. Two parameterizations of the aperture effects were then considered: permeability and transmission. Permeability values varied by an order of magnitude between the cases with an without apertures. However, transmission, the number of particles to leave the flow field in a given time, did not track with permeability. Despite having much greater permeability the regular aperture case permitted less particles to leave the flow than the regular case. Moreover, both the irregular cases had greater transmission values than the regular cases, a difference not supported by the permeability values. The travel time distributions of the particles were then used to try and understand the transmission results, however the findings were inconclusive. Overall, the findings of this study suggest that the effect of pore-scale apertures on flow though a pore-network may not be adequately captured by properties such as permeability for

applications that are interested in learning the time scales over which material may be transported and what volume of material was transported.

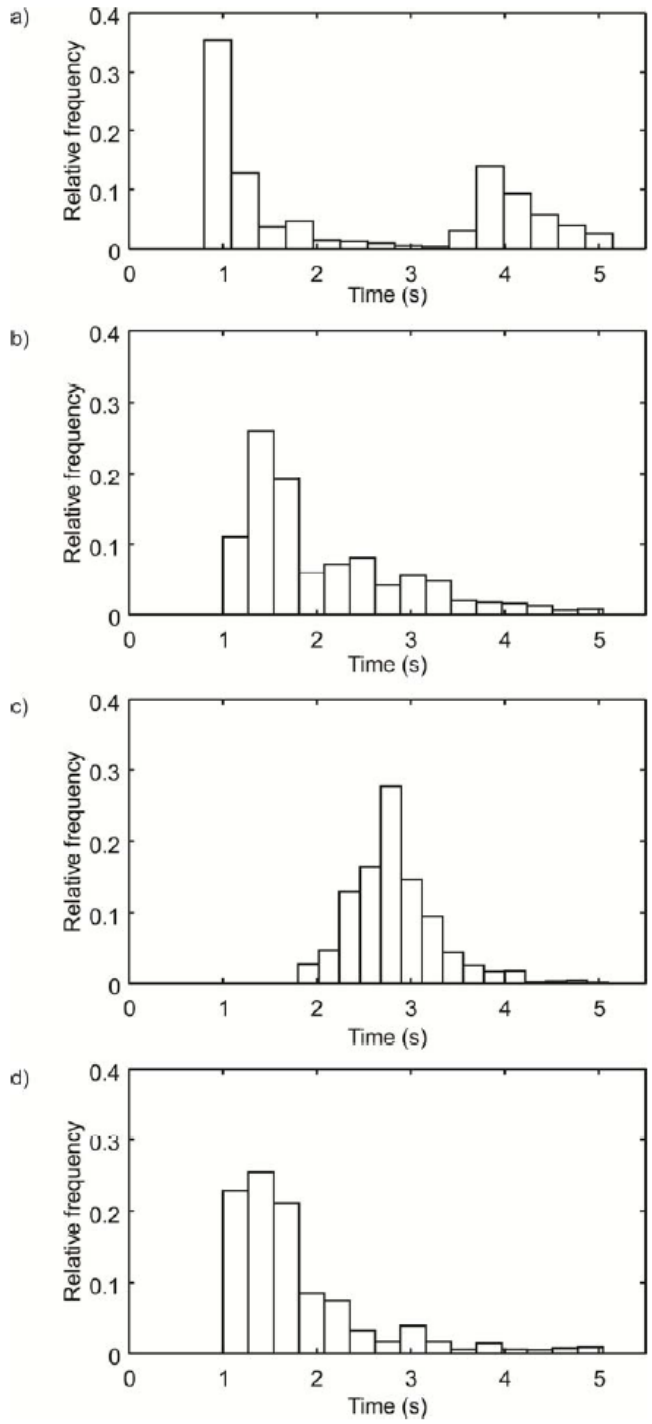

Figure 8 Travel times of the transmitted particles in the simulations for the (a) regular, (b) regular aperture, (c) irregular and (d) irregular aperture cases.

DISTRIBUTION

1	MS0404	Neill Symons	06752 (electronic copy)
1	MS1033	Scott Broome	08864 (electronic copy)
1	MS0899	Technical Library	9536 (electronic copy)


Sandia National Laboratories